2004

Structure of Shiga Toxin Type 2 (Stx2) from *Escherichia coli* O157:H7

Marie E. Fraser
University of Calgary

Masao Fujinaga
University of Alberta

Maia M. Cherney
University of Alberta

Angela R. Melton-Celsa
Uniformed Services University of the Health Sciences

Edda M. Twiddy
Uniformed Services University of the Health Sciences

See next page for additional authors

THE JOURNAL OF BIOLOGICAL CHEMISTRY Vol. 279, No. 26, Issue of June 25, pp. 27511–27517, 2004
Printed in U.S.A.

Structure of Shiga Toxin Type 2 (Stx2) from *Escherichia coli* O157:H7*

Received for publication, February 22, 2004, and in revised form, April 7, 2004
Published, JBC Papers in Press, April 9, 2004, DOI 10.1074/jbc.M401939200

Marie E. Fraser‡, Masao Fujinaga§, Maia M. Cherney§, Angela R. Melton-Celsa¶, Edda M. Twiddy¶, Alison D. O'Brien¶, and Michael N. G. James§‖

From the ‡Department of Biological Sciences, University of Calgary, Calgary, Alberta T2N 1N4, Canada, the §Canadian Institutes for Health Research Group in Protein Structure and Function, Department of Biochemistry, University of Alberta, Edmonton, Alberta T6G 2H7, Canada, and the ¶Department of Microbiology and Immunology, Uniformed Services University of the Health Sciences, Bethesda, Maryland 20814

Several serotypes of *Escherichia coli* produce protein toxins closely related to Shiga toxin (Stx) from *Shigella dysenteriae* serotype 1. These Stx-producing *E. coli* cause outbreaks of hemorrhagic colitis and hemolytic uremic syndrome in humans, with the latter being more likely if the *E. coli* produce Stx2 than if they only produce Stx1. To investigate the differences among the Stxs, which are all AB_5 toxins, the crystal structure of Stx2 from *E. coli* O157:H7 was determined at 1.8-Å resolution and compared with the known structure of Stx. Our major finding was that, in contrast to Stx, the active site of the A-subunit of Stx2 is accessible in the holotoxin, and a molecule of formic acid and a water molecule mimic the binding of the adenine base of the substrate. Further, the A-subunit adopts a different orientation with respect to the B-subunits in Stx2 than in Stx, due to interactions between the carboxyl termini of the B-subunits and neighboring regions of the A-subunit. Of the three types of receptor-binding sites in the B-pentamer, one has a different conformation in Stx2 than in Stx, and the carboxyl terminus of the A-subunit binds at another. Any of these structural differences might result in different mechanisms of action of the two toxins and the development of hemolytic uremic syndrome upon exposure to Stx2.

Several serotypes of *Escherichia coli* produce one or more protein toxins that are closely related to Stx from *Shigella dysenteriae* serotype 1 (1). Stx from *S. dysenteriae* was first identified by Kiyoshi Shiga for whom these toxins are named (2). Collectively these *E. coli* are known as Stx-producing *E. coli* (STEC).[1] *E. coli* O157:H7 is the STEC responsible for many outbreaks of hemorrhagic colitis or bloody diarrhea in the U.S., Canada, and Japan. In some patients the prodrome of hemorrhagic colitis may progress to the hemolytic uremic syndrome, which culminates in kidney failure. Two types of Stx may be produced by STEC, Stx1 and/or Stx2. The Stx types all have an AB_5 structure, in which a single A-subunit is associated with five B-subunits. The A-subunit embodies the *N*-glycosidase catalytic activity; it acts by removing a specific adenine base from the 28 S rRNA of the 60 S ribosomal subunit within infected cells. Because this adenine base is on a loop of rRNA that is important for elongation factor binding, the toxin is able to shut down protein synthesis in a targeted cell. The A-subunit of Stx1 is nearly identical to the A-subunit of Stx; it differs only by the change of a single serine residue at position 45 to a threonine (Table I). In contrast, the amino acid sequence identity between the A-subunits of Stx1 and Stx2 is only 55%. The B-pentamer of the Stxs contains the binding sites for glycolipids that are located on the surface of target cells, and thus mediates entry of the catalytic A-subunit into cells. Although the Stx1 group is homogeneous, the Stx2 group has a number of variants. Variants of Stx2 include Stx2c, Stx2d, Stx2d-activable, Stx2e, and Stx2f. Only the Stx2c variant of Stx2 has been found in the O157 serotypes. The Stx2 variants are distinguished by a difference in biological activity, immunological reactivity, or the receptor to which they bind. Stx1, Stx2, and the Stx2 variants bind preferentially to the glycosphingolipid globotriaosylceramide (Galα1–4Galβ1–4glucosyl ceramide, Gb_3) with the exception of Stx2e, which binds preferentially to globotetraosylceramide (GalNAcβ1–3Galα1–4Galβ1–4glucosyl ceramide). These different binding properties lead to the ability of the toxin to target different cells.

The molecular structure of the Stx1 B-pentamer alone was first determined using x-ray crystallography. This structure showed five B-subunits in a pentameric arrangement (3), similar to the arrangement of the B-subunits of the heat-labile enterotoxin (4). In heat-labile enterotoxin the five B-subunits surround a pore through which the carboxyl-terminal residues of the A-subunit traverse. When the structure of Stx was solved, the carboxyl-terminal tail of the A-subunit was found to be surrounded by its five B-subunits like heat-labile enterotoxin, whereas the remainder of the A-subunit lay on one side of the B-pentamer (5). The determinations of the structures of the Stx1 B-subunits and of their mutated forms, alone and in complex with sugars, have led to a better understanding of the binding properties of the B-pentamer (6–8) and have served as templates in the design of inhibitors to cell binding (9, 10).

The A-subunit of the Stxs can be proteolytically cleaved at a susceptible site (11), but the two portions, A1 (27.5 kDa) and A2 (4.5 kDa), remain covalently associated through a disulfide

* This work was supported in part by the National Institutes of Health (to A. D. O.), the Canadian Institutes of Health Research (to M. N. G. J.), the Natural Sciences and Engineering Research Council of Canada (to M. E. F.), and the Alberta Heritage Foundation for Medical Research (to M. E. F. and M. N. G. J.). The costs of publication of this article were defrayed in part by the payment of page charges. This article must therefore be hereby marked "*advertisement*" in accordance with 18 U.S.C. Section 1734 solely to indicate this fact.

The atomic coordinates and structure factors (codes 1R4P and 1R4Q) have been deposited in the Protein Data Bank, Research Collaboratory for Structural Bioinformatics, Rutgers University, New Brunswick, NJ (http://www.rcsb.org/).

‖ Awarded a Canada Research Chair in Protein Structure and Function. To whom correspondence should be addressed. Tel.: 780-492-4550; Fax: 780-492-0886; E-mail: Michael.James@ualberta.ca.

[1] The abbreviations used are: STEC, Stx-producing *E. coli*; Tris, Tris(hydroxymethyl)aminoethane; PPS, 3-(1-pyridino)-1-propanesulfonate; r.m.s., root mean square; Gb_3, globotriaosylceramide; MES, 4-morpholineethanesulfonic acid.

TABLE I
Sequence alignments of the A-subunits of Stx, Stx1, Stx2, ricin, and the B-subunits of Stx or Stx1 and Stx2

The sequence alignments were generated using ClustalW (39). For Stx, the sequence identifiers are CAA30741 and CAA30742 from Ref. 40; for Stx1 A, the sequence identifier is AAA98151 from Ref. 41; for Stx2, the sequence identifiers are CAA30714 and CAA30715 from Ref. 42.

```
Stx A          ----KEFTLDFSTAKTYVDSLNVIRSAIGTPLQTISSGGTSLLMIDSGTG 46
Stx1 A         ----KEFTLDFSTAKTYVDSLNVIRSAIGTPLQTISSGGTSLLMIDSGSG 46
Stx2 A         ----REFTIDFSTQQSYVSSLNSIRTEISTPLEHISQGTTSVSVINHTPP 46
Ricin A        IFPKQYPIINFTTAGATVQSYTNFIRAVRGRLTTGADVRHEIPVLPNRVG 50
                   :   ::*:*  : *.* . :   :   *   :.   .: ::

Stx A          DNLFAVDVRGIDPEEGRFNNLRLIVERNNLYVTGFVNRTNNVFYR----- 91
Stx1 A         DNLFAVDVRGIDPEEGRFNNLRLIVERNNLYVTGFVNRTNNVFYR----- 91
Stx2 A         GSYFAVDIRGLDVYQARFDHLRLIIEQNNLYVAGFVNTATNTFYR----- 91
Ricin A        -LPINQRFILVELSNHAELSVTLALDVTNAYVVGYRAGNSAYFFHPDNQE 99
                  :   .  ::  :     : * :: .* **.*:    .  *::

Stx A          -FADFSHVTFPGTTAVTLSGDSSYTTLQRVAGISRTGMQINRHSLTTSYL 140
Stx1 A         -FADFSHVTFPGTTAVTLSGDSSYTTLQRVAGISRTGMQINRHSLTTSYL 140
Stx2 A         -FSDFTHISVPGVTTVSMTTDSSYTTLQRVAALERSGMQISRHSLVSSYL 140
Ricin A        DAEAITHLFTDVQNRYTFAFGGNYDRLEQLAGNLRENIELGNGPLEEAIS 149
                  ::*:     .  ::: ...*  *:::*.  * .:::.. .*  :

Stx A          DLMSHS-GTSLTQSVARAMLRFVTVTAEALRFRQIQRGFRTTLDDLSGRS 189
Stx1 A         DLMSHS-GTSLTQSVARAMLRFVTVTAEALRFRQIQRGFRTTLDDLSGRS 189
Stx2 A         ALMEFS-GNTMTRDASRAVLRFVTVTAEALRFRQIQREFRQALSETAP-V 188
Ricin A        ALYYYSTGGTQLPTLARSFIICIQMISEAARFQYIEGEMRTRIRYNRR-- 197
                *  .* * :     :*:.:  : : :** **: *:  :*  :

Stx A          YVMTAEDVDLTLNWGRLSSVLPDYHGQDSVRVGRISFGSINAILGSVALI 239
Stx1 A         YVMTAEDVDLTLNWGRLSSVLPDYHGQDSVRVGRISFGSINAILGSVALI 239
Stx2 A         YTMTPGDVDLTLNWGRISNVLPEYRGEDGVRVGRISFNNISAILGTVAVI 238
Ricin A        SAPDPSVITLENSWGRLSTAIQESN--QGAFASPIQLQRRN---GSKFSV 242
                .  .  : *  .***:*..: : .  :.. .. *.:   .   *:   :

Stx A          LNCHHHASRVARMASDEFPSMCPADGRVRGITHNKILWDSSTLGAILMRR 289
Stx1 A         LNCHHHASRVARMASDEFPSMCPADGRVRGITHNKILWDSSTLGAILMRR 289
Stx2 A         LNCHHQGARSVRAVNEESQPECQITGDRPVIKINNTLWESNTAAAFLNRK 288
Ricin A        YDVSILIPIIALMVYRCAPPPSSQF------------------------- 267
                :     .  .  .     . .

Stx A          -----TISS 293
Stx1 A         -----TISS 293
Stx2 A         SQFLYTTGK 297
Ricin A        ---------

Stx/Stx1 B     TPDCVTGKVEYTKYNDDDTFTVKVGDKELFTNRWNLQSLLLSAQITGMTV 50
Stx2 B         -ADCAKGKIEFSKYNEDDTFTVKVDGKEYWTSRWNLQPLLQSAQLTGMTV 49
                .**..**:*::***:********..** :*.*****.** ***:*****

Stx/Stx1 B     TIKTNACHNGGGFSEVIFR-- 69
Stx2 B         TIKSSTCESGSGFAEVQFNND 70
               ***:.:*..*.**:** *.
```

bond until the two cysteine residues are reduced. The disulfide bond is between Cys-A241 and Cys-A260 in Stx2 (Table I). The amino acid residues forming the *N*-glycosidase catalytic site are on A1. The active site residues were initially predicted from the amino acid sequence similarity between A1 and the catalytic subunit of the toxin ricin found in castor beans (Table I) (12) and subsequently confirmed with genetic studies (summarized by Melton-Celsa and O'Brien (13)). The catalytic mechanism of ricin has been investigated in detail: the adenine base binds between two tyrosine side chains, Tyr-80 and Tyr-123, whereas Arg-180 is thought to act as an acid and Glu-177 either acts as a base to activate a water molecule or stabilizes the transition state (summarized in Ref. 14). In the structure of Stx, the disulfide bond connecting A1 and A2 is located near the residues that form the *N*-glycosidase active site; a methionine residue, only one residue away from the cysteine residue of A2, blocked access to the active site (5). Thus, the A-subunit in the holotoxin was predicted to be enzymatically inactive. The A2 peptide includes the carboxyl-terminal tail, which in the three-dimensional structure of Stx forms an α-helix surrounded by the five B-subunits. The carboxyl-terminal residues of A2 continue through the pore of the B-pentamer, but the last six residues appeared to be disordered in the Stx structure. This may result from the packing arrangement in the crystals, because two holotoxin molecules pack pentamer-to-pentamer, and these six residues would be located at this interface.

Despite their similar sequences and expected similar structures, Stx1 and Stx2 cause different degrees and types of tissue damage. If the *E. coli* O157:H7 with which a patient is infected produces mainly Stx2, the patient is more likely to suffer from hemolytic uremic syndrome than if the *E. coli* O157:H7 only produces Stx1 (summarized by Siegler *et al.* (15)). The difference in pathogenicity between strains that produce only Stx2 and those that produce Stx1 alone or Stx1 and Stx2 was postulated to be due to the greater affinity of the Stx1 B-pentamer for glycolipids (16). According to that theory, Stx1 would be more likely to be picked up by intestinal epithelial cells, where it could cause bloody diarrhea; Stx2 could then circulate through the bloodstream to the kidneys where it would cause the hemolytic uremic syndrome (17). However, both protein toxins produce effects in animals that do not appear to be due solely to targeting particular cell types (reviewed by O'Loughlin and Robins-Browne (1)). The tissue damage may be due to these other effects of the toxins and could be mediated by residues of the holotoxin that are not involved in receptor binding.

TABLE II
Statistics for the crystallographic data of Stx2

Space group	$P6_1$
Number of measurements	187,198
Number of unique reflections	66,898
Completeness (%) overall (1.86–1.80 Å)	98.3% (99.1%)
$I/\sigma I$ overall (1.86–1.80 Å)	8.0 (2.8)
R_{merge}[a] overall (1.86–1.80 Å)	6.0% (25.2%)

[a] $R_{merge} = \Sigma_{hkl}\Sigma_i|I - \langle I\rangle|/\Sigma_{hkl}\Sigma_i(I)$.

We have determined the structure of Stx2 and compared it to that of Stx to contribute to the understanding of what distinguishes Stx and Stx2 from each other. The experimental structures of the holotoxins can be used as templates upon which to model anti-infective compounds to treat the diseases caused by *E. coli* O157:H7 and other STECs. They can also be used to design chimera that could be used to decipher the different mechanisms of action of the two protein toxins in animal models.

EXPERIMENTAL PROCEDURES

Expression, Purification, and Crystallization of Stx2—Stx2 was produced in *E. coli* DH5α using the pLPSH3 plasmid and purified by immunoaffinity chromatography as previously described (13). The toxin eluted from the column with 0.1 M glycine, pH 7.8, and was dialyzed in TEAN (50 mM Tris, pH 7.5, with 1 mM EDTA, 3 mM sodium azide, and 0.2 M NaCl). SDS-PAGE analysis of the purified protein in the presence of the reducing agent, 2-mercaptoethanol, showed that the A-subunit was intact and had not been proteolyzed (data not shown).

Crystals of Stx2 were grown by vapor diffusion in hanging drops using sodium formate as the major precipitant. The drops were formed by mixing 1.5 μl of a 9.4 mg/ml solution of the protein with 1.5 μl of the reservoir solution. The reservoir solution contained 4 M sodium formate, 0.1 M MES (pH 6.0), 50 mM 3-(1-pyridino)-1-propanesulfonate (PPS), and 1% ethylene glycol. After a few days, crystals appeared as hexagonal bipyramids. These were seeded into fresh solutions where they grew to a maximum size of 0.35 mm by 0.30 mm within 3 weeks.

Structure Determination and Analysis—The crystals of Stx2 diffract to better than 1.8-Å resolution. For the data collection, one crystal was transferred to a solution containing 30% glycerol, 4 M sodium formate, 0.1 M MES (pH 6.0), and 1% ethylene glycol then vitrified at 100 K in the nitrogen stream of a Molecular Structure Corp. low temperature device. Diffraction data were collected from this crystal using a Raxis IV++ image plate detector mounted on a Rigaku RU-H3R rotating anode x-ray generator producing CuK_α radiation (λ = 1.5418 Å) that was monochromated and focused by Osmic mirrors. The data were processed using the programs DENZO and SCALEPACK (18). From the molecular weight, the unit cell dimensions, and the space group, the crystals were predicted to contain one AB_5-hexamer per asymmetric unit.

The structure was solved by the molecular replacement method using the programs ALMN (19) and BRUTE (20). The structure solution was performed in two stages, finding first the orientation and position

TABLE III
Statistics for the refined model of Stx2 and for the refined model of Stx

	Toxin type	
	Stx2	Stx
Resolution limit	1.77 Å	2.5 Å
Cell dimensions	$a = b = 143.96$ Å, $c = 59.30$ Å $\alpha = \beta = 90°$, $\gamma = 120°$	$a = 133.00$ Å $b = 147.18$ Å $c = 82.85$ Å $\alpha = \beta = \gamma = 90°$
Number of data for refinement	66,890	53,527
Completeness	97.6%	93.9%
R-factor (number of data)	15.1% (63,514)	19.9% (50,780)
R free (number of data)	18.4% (3,376)	25.7% (2,747)
Number of protein atoms	4,981	9,687
Number of water molecules	511	46
Number of atoms in ions or ligands	125	0
r.m.s. deviations from ideal geometry		
Bond lengths (Å)	0.017	0.016
Bond angles (°)	2.0	1.9
Ramachandran plot		
Number in most favored regions	522 (92.6%)	934 (85.8%)
Number in additional allowed regions	42 (7.4%)	147 (13.5%)
Number in generously allowed regions	0	6 (0.6%)
Number in disallowed regions	0	1 (0.1%)

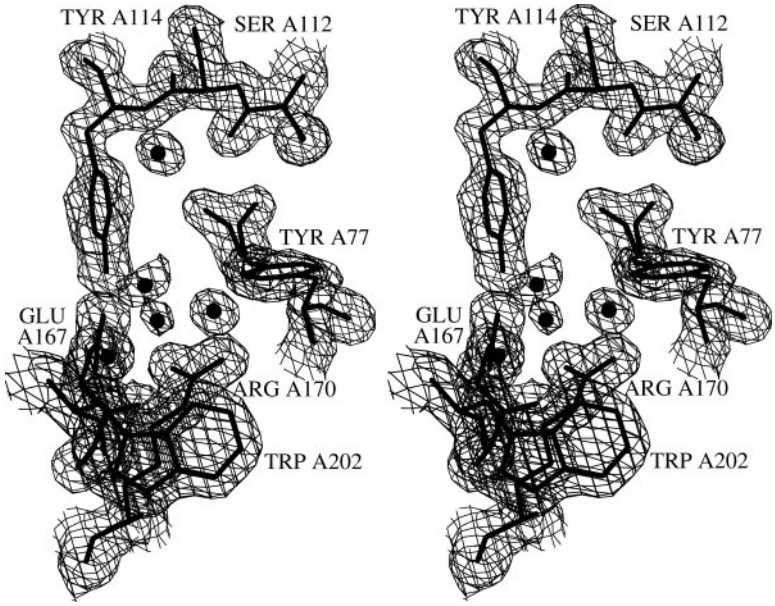

FIG. 1. **Electron density for Stx2.** The electron density from the $2F_o - F_c$, α_c map is contoured at 1σ near residues forming the active site. The molecular model is drawn as *sticks*, with water molecules depicted as *filled circles*. This figure was drawn with the programs BOBSCRIPT and MOLSCRIPT (35, 36).

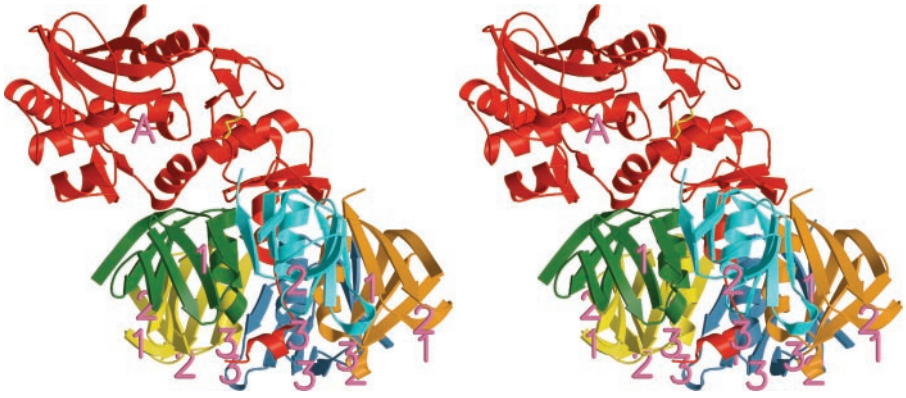

FIG. 2. **Ribbon diagram of Stx2.** The A-subunit is *red*, whereas the B-subunits are *orange* (chain B), *cyan* (chain C), *green* (chain D), *yellow* (chain E), and *blue* (chain F). The active site in the A-subunit is marked by the *magenta letter A*. The side chains of the cysteine residues that link A1 and A2 are depicted in *yellow*. The sites equivalent to the Gb_3-binding sites on the B-pentamer of Stx1 are shown by *magenta numbers* that distinguish the type of binding site (6). This figure and Figs. 6 and 7 were drawn with the programs MOLSCRIPT and RASTER3D (35, 37).

of the B-pentamer in the asymmetric unit and, subsequently, the orientation and location of the A-subunit. The search model for the B-pentamer was the structure of a mutant form of Stx2e (8), identified as 2BOS in the Protein Data Bank (21). The rotation function for the B-pentamer gave five peaks as expected, and the translation function clearly showed that the space group was $P6_1$. The search model for the

A-subunit was the A-subunit of Stx (5), using chain A of the structure identified as 1DM0 in the Protein Data Bank (21). The model was improved by cycles of maximum likelihood refinement using the Crystallography and NMR System (22) and model building using the molecular graphics programs XFIT (23) and TOM/FRODO (24). The quality of the model was judged with information from the programs PROCHECK (25) and WHATCHECK (26), and the final unit cell dimensions were those suggested by WHATCHECK.

The structure of Stx had been determined at lower resolution (2.5 Å) (27) than that of Stx2 (1.77 Å), so we hypothesized that the model for Stx could be improved by using information from the structure of Stx2. As well, Stx had been refined prior to the use of the maximum likelihood target in refinement (28). For these reasons, the Stx model was refined for several additional cycles using the original data set (5). The final refined structures of Stx and Stx2 were analyzed and compared using programs from the CCP4 package (19) as well as the molecular graphics programs O (29) and Swiss PDB Viewer (30). The atomic coordinates and the structure factors for both Stx2 and Stx have been deposited in the Protein Data Bank (21), where they have been assigned the identifiers 1R4P for Stx2 and 1R4Q for Stx.

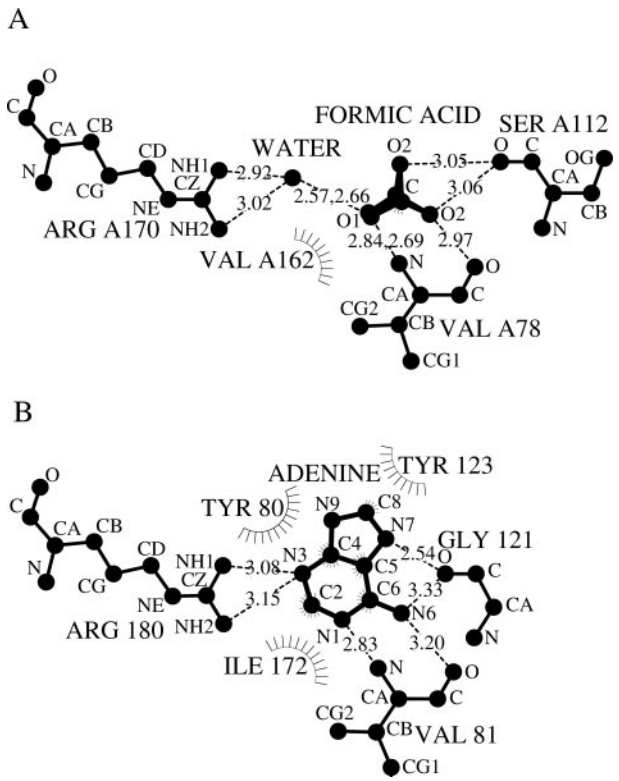

FIG. 3. **Active site of Stx2 (*A*) and ricin (*B*).** *Dashed lines* represent hydrogen bonding interactions, and the interatomic distances are noted. *A*, configuration of the two alternate conformations of formic acid and a water molecule in the active site of Stx2. *B*, adenine bound to the A chain of ricin (31). This figure was drawn using the program LIGPLOT (38).

RESULTS

Stx2—Table II presents the crystallographic details for Stx2, and Table III presents the statistics from the refinement. This is a well determined structure, as demonstrated by the low values of the *R*-factors and the excellent geometry of the refined model. The catalytic site of the A-subunit of Stx2 is accessible in the crystal structure, and Fig. 1 shows that it contains electron density. Three water molecules could be modeled into this electron density, and their positions and temperature factors were refined. The distances from these water molecules to atoms of the protein were reasonable hydrogen bonding distances, but the three were too close to each other for hydrogen-bonding (2.0, 2.1, and 2.2 Å). Instead, for the final model, a molecule of formic acid (used to crystallize the protein) has been modeled in two alternate conformations to account for the electron density. The crystal structure of Stx2 shows that most of the A-subunit is located on one side of the B-pentamer, but residues of A2 traverse the pore of the B-pentamer and form a short helix on the cell surface binding side (see Fig. 2). In the pore, residues of the A2 portion of Stx2 begin in an α-helical conformation (residues Ser-A278 to Leu-A285), changing to an extended conformation from Asn-A286 to Ser-A289. (The nomenclature indicates the amino acid residue followed by the chain letter and the position of the amino acid residue in that chain.) Ser-A289 initiates the final helix near the carboxyl terminus of the A-subunit. This terminal helix projects out of the B-pentamer pore at an angle of about 30° to the base of the B-pentamer and packs alongside two of the B-subunits. The final two residues of the A-subunit (Gly-A296 and Lys-A297) are not part of the helix, but they are well ordered in the structure.

Stx—We next took the information from the structure of Stx2 and refined further the structure of Stx. The new refinement improved the electron density in some regions, notably residues 43–46 and 184–188 of the A-subunit. Two and three additional residues could be fit at the carboxyl termini of A1 and A2, respectively, but the remaining carboxyl-terminal residues are disordered in the crystal structure. Data for the newly refined model for Stx are included in Table II.

DISCUSSION

Active Site of Stx2—The active site of the A subunit is accessible in Stx2 in contrast to the active site of the A subunit in Stx. In the crystal structure of Stx2, a molecule of formic acid and a water molecule bound in the active site mimic the binding of adenine (Fig. 3). The water molecule interacting with Arg-A170 closely approximates the position of N3 of adenine when bound to ricin (31). The oxygen atoms of formic acid occupy roughly the positions of N1 and N6 or N1 and N7 of the adenine in the two alternate orientations of the molecule of formic acid, and the carbon atom approximates the position of C6 of adenine. The tyrosine residue (residue A77) that forms part of the catalytic site is in a different conformation in Stx

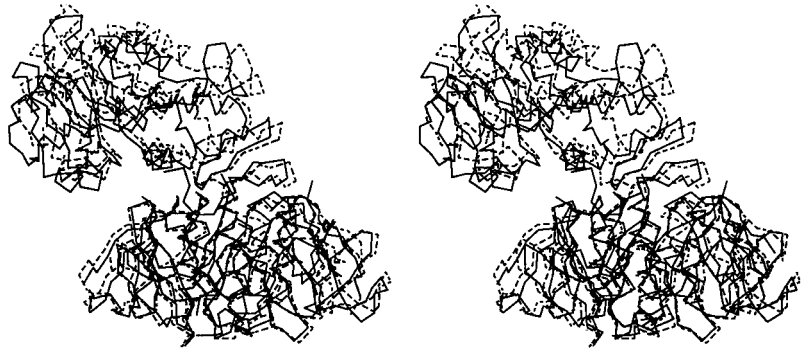

FIG. 4. **Cα trace of Stx2 superposed on that of Stx.** Stx2 is shown in *solid lines*, whereas Stx is shown in *dashed lines* in this stereoview. The superposition was based solely on structurally equivalent residues of the B-pentamers. This figure and Fig. 5 were drawn with the program MOLSCRIPT (35).

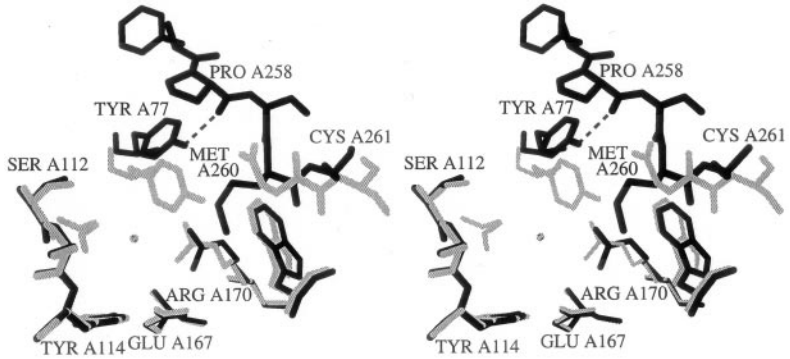

FIG. 5. **Active sites of Stx2 and Stx.** In this stereoview, residues of Stx2 are drawn as *gray stick models*, whereas residues of Stx are drawn in *black*. Specific residues of Stx are labeled. The hydrogen bonding interaction between the active site tyrosine residue, Tyr-A77, and the carbonyl oxygen atom of Pro-A258 is represented by a *dashed line*. Residues Ala-257 to Ala-261 are the part of A2 that lies across the active site.

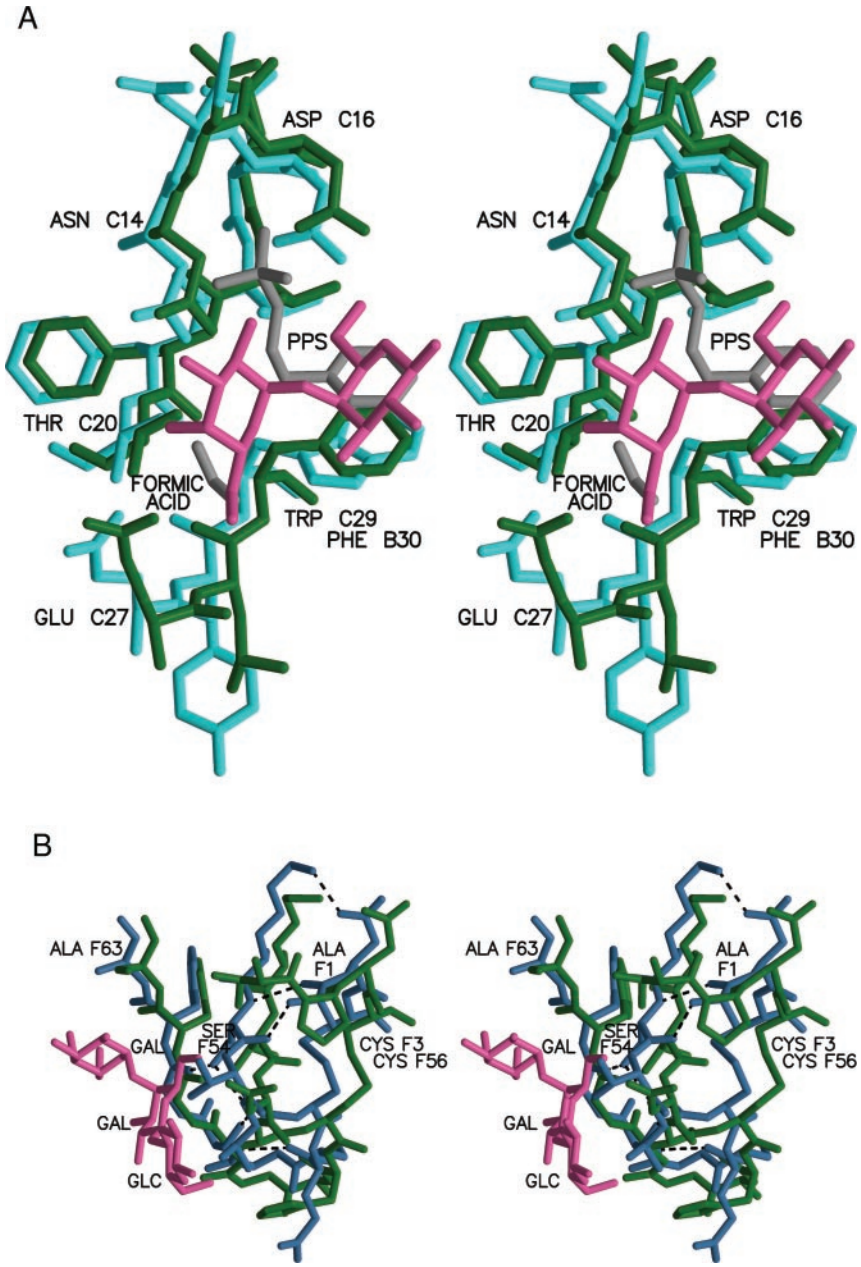

FIG. 6. **Receptor-binding sites 1 and 2.** *A*, PPS and formic acid, drawn as *gray stick models* in this stereoview, bind to the site in Stx2 (*cyan*, chain C) that is equivalent to the type 1 binding site for the Gb_3 analogue (*magenta*) on the B-pentamer of Stx1 (*green*, chain B) (6). *B*, this stereoview shows that the loop that binds the Gb_3 analogue (*magenta*) at site 2 of the B-pentamer of Stx1 (*green*, chain F) has a different conformation than the equivalent loop in Stx2 (*blue*, chain F) (6). Hydrogen bonding interactions in Stx2 are shown by *dashed lines*.

and Stx2, as well as in the structures of ricin alone and in ricin when complexed with adenine. The different conformations of the tyrosine residue in these active sites indicate that this tyrosine side chain could adopt different conformations during a catalytic cycle. The role of the tyrosine residue in catalysis is most likely to bind the substrate by stacking with the adenine

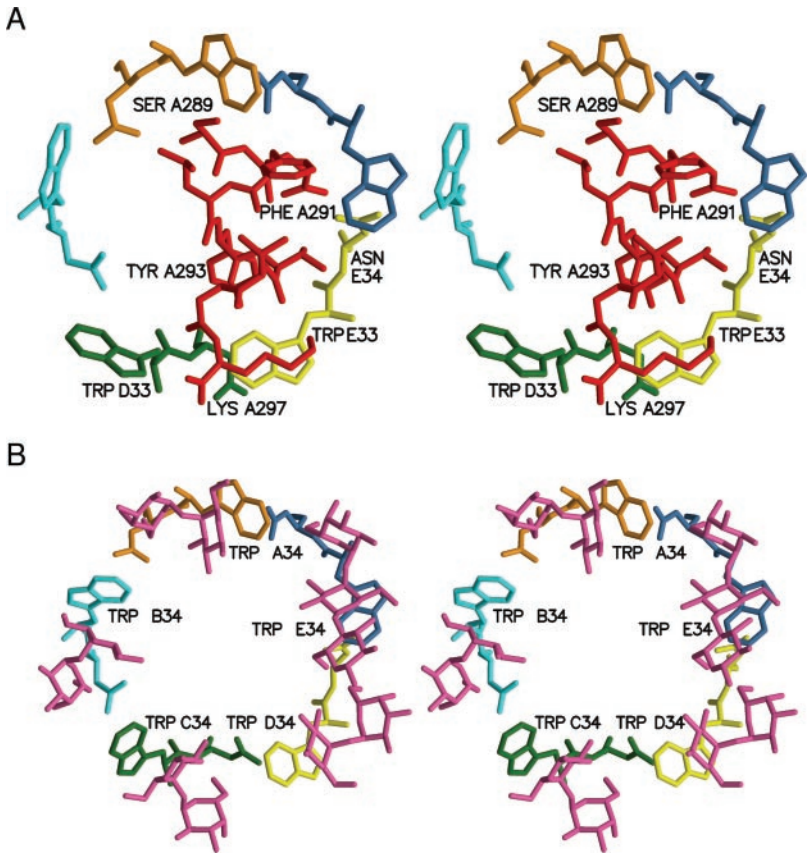

FIG. 7. **Receptor-binding site 3.** *A*, the tail of the A subunit (*red*) protrudes from the base of the B-pentamer in Stx2, as shown in this stereoview. The five pairs of tryptophan and asparagine residues at the base of the B-pentamer (*shaded* according to the chain identifier as in Fig. 2) adopt different conformations. *B*, In the structure of the Gb_3 analogue bound to the B-pentamer of Stx, the equivalent residues have similar conformations for all five type 3 binding sites (6).

ring. However, in the structure of Stx, this tyrosine residue forms a hydrogen bond through its hydroxyl group with the carbonyl oxygen atom of Pro-A258, one of the residues of A2. It is this stretch of A2 that lies across the active site of Stx, as shown in Fig. 4.

Superpositions of Stx2 and Stx—The orientation of the A-subunit with respect to the B-pentamer differs in the two holotoxins Stx2 and Stx. Fig. 5 shows the superposition of the two holotoxins using only residues of the B-pentamers to align the structures, which superpose with an r.m.s. deviation of 1.3 Å for the 340 Cα atoms. The A-subunits superpose with an r.m.s. deviation of 0.84 Å for 246 Cα atoms. The sequences of the A-subunits are most different in the region of the cleavage loop and in the stretch of polypeptide following the second cysteine residue. The B-subunits of Stx2 are two residues longer at the carboxyl terminus than the B-subunits of Stx; in both toxins, the carboxyl-terminal residues of the B-subunits interact with the A-subunit. These different specific interactions may be responsible for the different orientations of the A-subunits with respect to their B-pentamers in the holotoxins.

Comparison of the Receptor-binding Sites—Three distinct receptor-binding sites have been identified on the B-pentamer of Stxs (6). Fig. 2 shows the locations of the equivalent sites on Stx2.

Carbohydrate Binding Site 1—Receptor binding site 1 is located in a groove formed by two B-subunits where they interact to create the seven-stranded β-sheet. A molecule of 3-(1-pyridino)-1-propanesulfonate (PPS) is bound to Stx2 in four of the five potential type 1 binding sites. Fig. 6*A* demonstrates how the phenyl ring of PPS stacks against the indole ring of Trp-C29, mimicking the binding of the second galactose ring of the carbohydrate with the phenyl ring of Phe-30 of the B-subunit of Stx1. In the fifth unoccupied type 1 binding site, the side chain of Glu-A184 from a crystallographically related hexamer packs close enough to Trp-E29 to occlude the PPS-binding site. Two of the type 1 binding sites that do bind PPS also contain a molecule of formic acid that partially mimics the binding of the first galactose ring of the carbohydrate. The sulfonate group of each molecule of PPS also interacts with the B-pentamer, primarily via a water molecule that forms a link to Glu-15 of the B-subunit and to the side chain of Glu-64 of the neighboring B-subunit. This interaction could be exploited in the design of anti-infectives that would bind to site 1.

Carbohydrate Binding Site 2—The conformation of Stx2 at the type 2 binding site differs from that of Stx, and the differences in both the sequences and the conformations are likely to lead to the different binding affinities for Gb_3. The first residue of the B-subunit of Stx2 is alanine, which aligns with Pro-2 of the B-subunit of Stx. The NH_3^+ group of Ala-1 forms a hydrogen bond to the carbonyl oxygen atom of Ser-B53, leading to a different conformation in the loop to which the carbohydrate binds (Fig. 6*B*). The disulfide bond between cysteine residues B3 and B56 of Stx2 adopts a conformation different from that of the disulfide link between residues B4 and B57 of Stx1. For Gb_3 to bind to Stx2 in the same way that the Gb_3 analogue binds to the B-pentamer of Stx1, there would have to be a change in the conformation of this disulfide-bridged loop, otherwise the carbohydrate would clash with Ser-B54.

Carbohydrate Binding Site 3—The type 3 binding site is at the base of the pentamer, where the tail of A2 emerges from the B-pentamer pore in Stx2. The final two residues of A2 pack against one of the tryptophan residues that have been shown to be crucial for the binding of Gb_3 at this lower affinity site (7, 32). In Stx2, the five tryptophan rings (residue 33 in each B-subunit) all have clear electron density, but they do not adopt a common conformation (Fig. 7*A*); whereas in the complex of a Gb_3 analogue with the B-pentamer of Stx1, all five tryptophan side chains have similar conformations (Fig. 7*B*) (6). To bind Gb_3 at site 3, it may be necessary for all five binding sites to be available, so that the tryptophan and the adjacent asparagine

side chains are able to move in concert to the binding conformation. This view is supported by the structure of a mutated form of the Stx2e B-pentamer with the Gb_3 analogue, in which the carbohydrate is seen to bind to sites 1 and 2, but, surprisingly, not to site 3 (8). In the crystals of this mutated Stx2e B-pentamer in complex with the Gb_3 analogue, an interaction with a crystallographically related molecule causes one of the tryptophan side chains to adopt a specific conformation that is different from that in the complex of the B-pentamer of Stx1 with Gb_3.

Roles for the Structural Differences in the Pathogenicity of Stx2—Four major differences between the structures of Stx and Stx2 were found in this study. First, the active site of Stx2 is accessible in the crystal structure, in contrast to the active site of Stx that is blocked by part of the polypeptide chain of A2. This greater accessibility of the Stx2 active site may contribute to the apparently greater pathogenicity of Stx2 as compared with Stx. It also means that inhibitors directed to the active site of the *N*-glycosidase could bind to the Stx2 holotoxin in the extracellular environment and enter the target cell in complex with the holotoxin. Within the cell, these inhibitors would prevent the toxin from shutting down protein synthesis. Second, the carboxyl terminus of the Stx2 A-subunit forms a short 2-turn α-helix after threading through the pore of the B-pentamer, in contrast to the tail of the Stx A-subunit, which in the crystals shows disorder in the same region. The carboxyl-terminal tail of the Stx2d-activable A2 has been shown to be involved in the enhanced toxicity of Stx2d-activable in the presence of elastase from mucus (33, 34). Perhaps the more ordered and extended structure found in the terminus of the Stx2 A2, could, by analogy, also be found in Stx2d-activable, and contribute to the accessibility of that peptide to elastase, which cleaves the terminal two amino acids from the A2 carboxyl terminus (34). Third, one of the receptor binding sites in the Stx2 B-pentamer has a different conformation than found in the Stx B-pentamer, and that different conformation may contribute to the different affinities of the two B-pentamers for Gb_3. Finally, the carboxyl terminus of the A1 peptide of Stx2 binds at one of the "receptor-binding" sites in Stx2, whereas that site is unoccupied in Stx, a finding that, again, may partially explain the different affinities of Stx and Stx2 for Gb_3.

Acknowledgment—M. N. G. J. acknowledges with thanks the award of a Canada Research Chair.

REFERENCES

1. O'Loughlin, E. V., and Robins-Browne, R. M. (2001) *Microbes Infection* **3,** 493–507
2. Shiga, K. (1898) *Zentralbl. Bakteriol. Orig.* **24,** 913–918
3. Stein, P. E., Boodhoo, A., Tyrrell, G. J., Brunton, J. L., and Read, R. J. (1992) *Nature* **355,** 748–750
4. Sixma, T. K., Pronk, S. E., Kalk, K. H., Wartna, E. S., van Zanten, B. A. M., Witholt, B., and Hol, W. G. J. (1991) *Nature* **351,** 371–377
5. Fraser, M. E., Chernaia, M. M., Kozlov, Y. V., and James, M. N. (1994) *Nat. Struct. Biol.* **1,** 59–64
6. Ling, H., Boodhoo, A., Hazes, B., Cummings, M. D., Armstrong, G. D., Brunton, J. L., and Read, R. J. (1998) *Biochemistry* **37,** 1777–1788
7. Ling, H. (1999) *Structural Studies of the Interactions between Shiga-like Toxins and their Carbohydrate Receptor*. Ph.D. thesis, Department of Biochemistry, pp. 185, University of Alberta, Edmonton, Alberta
8. Ling, H., Pannu, N. S., Boodhoo, A., Armstrong, G. D., Clark, C. G., Brunton, J. L., and Read, R. J. (2000) *Structure* **8,** 253–264
9. Kitov, P. I., Sadowska, J. M., Mulvey, G., Armstrong, G. D., Ling, H., Pannu, N. S., Read, R. J., and Bundle, D. R. (2000) *Nature* **403,** 669–672
10. Mulvey, G. L., Marcato, P., Kitov, P. I., Sadowska, J., Bundle, D. R., and Armstrong, G. D. (2003) *J. Infect. Dis.* **187,** 640–649
11. Olsnes, S., Reisbig, R., and Eiklid, K. (1981) *J. Biol. Chem.* **256,** 8732–8738
12. Ready, M., Katzin, B., and Robertus, J. (1988) *Proteins* **3,** 53–59
13. Melton-Celsa, A. R., and O'Brien, A. D. (2000) in *Handbook of Experimental Pharmacology* (Aktories, K., and Just, I., eds) pp. 385–406, Springer, Freiburg
14. Miller, D. J., Ravikumar, K., Shen, H., Suh, J.-K., Kerwin, S. M., and Robertus, J. D. (2002) *J. Med. Chem.* **45,** 90–98
15. Siegler, R. L., Obrig, T. G., Pysher, T. J., Tesh, V. L., Denkers, N. D., and Taylor, F. B. (2003) *Pediatr. Nephrol.* **18,** 92–96
16. Head, S. C., Karmali, M. A., and Lingwood, C. A. (1991) *J. Biol. Chem.* **266,** 3617–3621
17. Tesh, V. L., Burris, J. A., Owens, J. W., Gordon, V. M., Wadolkowski, E. A., O'Brien, A. D., and Samuel, J. E. (1993) *Inf. Immun.* **61,** 3392–3402
18. Otwinowski, Z., and Minor, W. (1997) *Methods Enzymol.* **276,** 307–326
19. Collaborative Computational Project, N. (1994) *Acta Crystallogr. Sect. D Biol. Crystallogr.* **50,** 760–763
20. Fujinaga, M., and Read, R. J. (1987) *J. Appl. Crystallogr.* **20,** 517–521
21. Berman, H. M., Westbrook, J., Feng, Z., Gilliland, G., Bhat, T. N., Weissig, H., Shindyalov, I. N., and Bourne, P. E. (2000) *Nucleic Acids Res.* **28,** 235–242
22. Brunger, A. T., Adams, P. D., Clore, G. M., Delano, W. L., Gros, P., Grosse-Kunstleve, R. W., Jiang, J.-S., Kuszewski, J., Jilges, N., Pannu, N. S., Read, R. J., Rice, L. M., Simonson, T., and Warren, G. L. (1998) *Acta Crystallogr. Sect. D Biol. Crystallogr.* **54,** 905–921
23. McRee, D. E. (1999) *J. Struct. Biol.* **125,** 156–165
24. Jones, T. A. (1985) *Methods Enzymol.* **115,** 157–171
25. Laskowski, R. A., MacArthur, M. W., Moss, D. S., and Thornton, J. M. (1993) *J. Appl. Crystallogr.* **26,** 283–291
26. Hooft, R. W. W., Vriend, G., Sander, C., and Abola, E. E. (1996) *Nature* **381,** 272
27. Fraser, M. E., Chernaia, M. M., Kozlov, Y. V., and James, M. N. G. (1996) in *Protein Toxin Structure* (Parker, M. W., ed) pp. 173–190, Springer, Heidelberg
28. Pannu, N. S., and Read, R. J. (1996) *Acta Crystallogr. Sect. A* **52,** 659–668
29. Jones, T. A., Zou, J. Y., Cowan, S. W., and Kjeldgaard, M. (1991) *Acta Crystallogr. Sect. A* **47,** 110–119
30. Guex, N., and Peitsch, M. C. (1997) *Electrophoresis* **18,** 2714–2723
31. Weston, S. A., Tucker, A. D., Thatcher, D. R., Derbyshire, D. J., and Pauptit, R. A. (1994) *J. Mol. Biol.* **244,** 410–422
32. Bast, D. J., Banerjee, L., Clark, C., Read, R. J., and Brunton, J. L. (1999) *Mol. Microbiol.* **32,** 953–960
33. Kokai-Kun, J. F., Melton-Celsa, A. R., and O'Brien, A. D. (2000) *J. Biol. Chem.* **275,** 3713–3721
34. Melton-Celsa, A. R., Kokai-Kun, J. F., and O'Brien, A. D. (2002) *Mol. Microbiol.* **43,** 207–215
35. Kraulis, P. J. (1991) *J. Appl. Crystallogr.* **24,** 946–950
36. Esnouf, R. M. (1997) *J. Mol. Graphics* **15,** 132–134
37. Merritt, E. A., and Bacon, D. J. (1997) *Methods Enzymol.* **277,** 505–524
38. Wallace, A. C., Laskowski, R. A., and Thornton, J. M. (1995) *Prot. Eng.* **8,** 127–134
39. Thompson, J. D., Higgins, D. G., and Gibson, T. J. (1994) *Nucleic Acids Res.* **22,** 4673–4680
40. Kozlov, Y. V., Kabishev, A. A., Fedchenko, V. I., and Baev, A. A. (1987) *Dokl. Biochem.* **295,** 740–744
41. Jackson, M. P., Newland, J. W., Holmes, R. K., and O'Brien, A. D. (1987) *Microb. Pathog.* **2,** 147–153
42. Jackson, M. P., Neill, R. J., O'Brien, A. D., Holmes, R. K., and Newland, J. W. (1987) *FEMS Microbiol. Lett.* **44,** 109–114

ADDITIONS AND CORRECTIONS

This paper is available online at www.jbc.org

THE JOURNAL OF BIOLOGICAL CHEMISTRY VOL. 281, NO. 51, p. 39740, December 22, 2006

VOLUME 279 (2004) PAGES 27511–27517

Structure of Shiga toxin type 2 (Stx2) from *Escherichia coli* O157:H7.

Marie E. Fraser, Masao Fujinaga, Maia M. Cherney, Angela R. Melton-Celsa, Edda M. Twiddy, Alison D. O'Brien, and Michael N. G. James

PAGE 27512:

Under "Experimental Procedures," subheading "Expression, Purification, and Crystallization of Stx2," the name of the plasmid in the first sentence should be "pJES120." The sentence, therefore, should read: "Stx2 was produced in *E. coli* DH5α using the pJES120 plasmid. . . . "

VOLUME 281 (2006) PAGES 33078–33086

The marine product cephalostatin 1 activates an endoplasmic reticulum stress-specific and apoptosome-independent apoptotic signaling pathway.

Nancy López-Antón, Anita Rudy, Nicole Barth, M. Lienhard Schmitz, George R. Pettit, Klaus Schulze-Osthoff, Verena M. Dirsch, and Angelika M. Vollmar

Dr. Schmitz's name did not appear in the proper order. The correct spelling and order of his name is shown above.